Journal of Inorganic Biochemistry 191 (2019) 1–7

Contents lists available at ScienceDirect

Journal of Inorganic Biochemistry

journal homepage: www.elsevier.com/locate/jinorgbio

# Structure-activity relationships for highly potent half-sandwich organoiridium(III) anticancer complexes with CˆN-chelated ligands

Yuliang Yang[a], Lihua Guo[a,*], Xingxing Ge[a], Shaopeng Shi[a], Yuteng Gong[a], Zhishan Xu[a,b], Xiaofeng Zheng[a], Zhe Liu[a,*]

[a] Institute of Anticancer Agents Development and Theranostic Application, The Key Laboratory of Life-Organic Analysis and Key Laboratory of Pharmaceutical Intermediates and Analysis of Natural Medicine, Department of Chemistry and Chemical Engineering, Qufu Normal University, Qufu 273165, China
[b] Department of Chemistry and Chemical Engineering, Shandong Normal University, Jinan 250014, China

ARTICLE INFO

*Keywords:*
Imine-N-heterocyclic carbene
Half-sandwich
Iridium(III) complexes
Structure-activity relationships
Anticancer

ABSTRACT

We herein report the synthesis, characterization, catalytic ability in converting coenzyme NADH to $NAD^+$ and anticancer activity of half-sandwich iridium(III) complexes, $[(\eta^5\text{-}Cp^{xbiph})Ir(C\text{^}N)Cl]PF_6$, where $Cp^{xbiph}$ = tetramethyl(biphenyl)cyclopentadienyl, CˆN = varying imine-N-heterocyclic carbene ligands. The molecular structure of $[(\eta^5\text{-}Cp^{xbiph})Ir(L6)Cl]PF_6$ (complex **Ir6**), exhibiting the familiar "piano-stool" geometry, has been authenticated by X-ray crystallography. The anticancer activities of these complexes can be governed via substituent effects of three tunable domains and the ligand substituted variants offer an effective chelate ligand set that distinguishes anticancer activity and catalytic ability. Notably, complex **Ir6** displays the greatest cytotoxic activities ($IC_{50}$ = 0.85 μM), whose anticancer activity is more approximately 25-fold higher than that of cisplatin. The initial cell death mechanistic insight displays that this group of iridium(III) complexes exerts anticancer effects via cell cycle arrest, apoptosis induction and loss of the mitochondrial membrane potential. In addition, the confocal microscopy imaging shows that the complex **Ir6** can damage lysosome. Overall, preliminary structure–activity relationships study and understanding of the cell death mechanism perhaps provide a rational strategy for enhancing anticancer activity of this family of complexes.

## 1. Introduction

Since cancer has an increasing impact on mortality worldwide, a growing number of researchers are being devoted to the exploration of emerging cancer therapy strategies. Among these, cytotoxic chemotherapeutic agents play a vital role in fighting cancer. Platinum-based complexes are represented by cisplatin, which are extensively employed for the treatment of a wide range of tumors [1–3]. At present, > 50% of chemotherapy treatments involve the use of platinum drugs. However, patients receiving these agents have suffered severe adverse effects, including nephrotoxicity, myelosuppression, peripheral neuropathy, ototoxicity, and nausea, which limits the dose that can be administered [4–7]. Therefore, the investigation of other metal-based anticancer agents as promising candidates and alternative drugs to cisplatin and its derivatives containing highly anticancer efficacy, low-toxicity and low side effects in normal tissues has received a significant amount of attention [8,9].

Organometallic compounds, which provide a potentially unexplored field for biological and medicinal application, recently attract increasing interest in the field of bioorganometallic chemistry [10–24]. In particular, metal complexes ligated by N-heterocyclic carbenes (NHCs) have found wide applications in various fields, particularly as catalysts and anticancer agents [25–33]. At present, various transition metal complexes, including Pt, Os, Pd, Ag, Au, Ru, Rh and Ir have been explored as novel cancer treatment options [34–39]. For example, Che et al. reported a panel of cyclometalated palladium(II) N-heterocyclic carbene compounds (**I**, Scheme 1) and explored their reaction with biomolecules glutathione (GSH), ascorbic acid and human serum albumin (HSA) [34]. The mechanisms of action (MoAs) of this class of complexes were studied via different analysis assays, including mitochondrial membrane depolarization and inhibition of epidermal growth factor receptor (EGFR) signaling pathway in association with apoptotic cell death of the cancer cells. Similarly, Mao's group developed a family of mitochondria-targeted Ag(I)- and Au(I)-NHC anticancer agents bearing imidazolium-linked cyclophanes, which showed potent cytotoxicity toward cancer cell lines (**II**, Scheme 1) [35]. The selectivity, stable in aqueous solutions and cell death mechanism of these complexes can be remarkably distinguished via alternative metal

* Corresponding authors.
*E-mail addresses:* guolihua@qfnu.edu.cn (L. Guo), liuzheqd@163.com (Z. Liu).

https://doi.org/10.1016/j.jinorgbio.2018.11.007
Received 1 September 2018; Received in revised form 16 October 2018; Accepted 8 November 2018
Available online 10 November 2018
0162-0134/ 

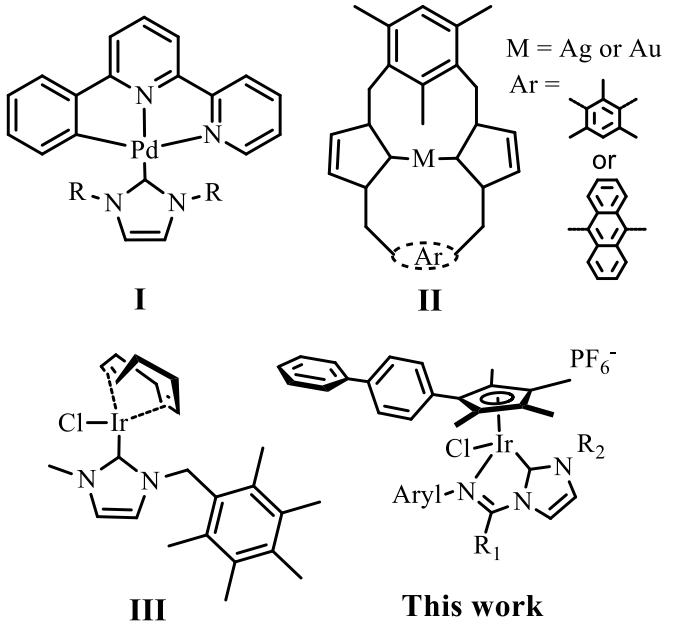


**Scheme 1.** Reported N-heterocyclic carbene anticancer complexes and our current work.

ions. In addition, a new series of iridium(I)-NHC complex has been prepared by Metzler-Nolte et al. (**III**, Scheme 1) [36]. This complex showed high cytotoxicity against three different cancer cell lines, which is attributed to an unusual oxidative mechanism. Numerous metal-NHC complexes have emerged as promising antitumor agents, but only a few iridium-NHC anticancer agents have been limitedly developed. These investigations motivated us to design new type of half-sandwich iridium (III) complexes bearing imine-N-heterocyclic carbene ligands and explore their possible anticancer mechanisms.

In this study, a series of structurally analogous half-sandwich iridium(III) complexes with similar structure $[(\eta^5\text{-Cp}^{xbiph})\text{Ir(C^N)Cl}]PF_6^-$ were successfully synthesized and systematically studied for chemical and biological activities, mainly including catalytic potential in oxidize NADH to $NAD^+$, in vitro cytotoxic activity toward A549 cancer cells and their possible anticancer mechanisms. Specially, the structural–activity relationships (SARs) of anticancer activity and catalytic potential in converting coenzyme NADH to $NAD^+$ of the complexes were adequately studied. The cell death mechanism, including arresting cell cycle, inducing apoptosis, dropping mitochondrial membrane potential (MMP) and the increase of lysosomal permeabilization, is also studied.

## 2. Results and discussion

### 2.1. Synthesis and characterization

The imidazolium salts (C^imine·HCl) (**L1–L6**) were prepared by reaction of corresponding imidoyl chlorides with N-substituted imidazole (Scheme 2). The synthetic route of the iridium(III) complexes in this work is depicted in Scheme 3. Complexes **Ir1–Ir6** with various imine-N-heterocyclic carbene ligands were obtained in moderate to high yields (55–88%) by corresponding silver NHC complexes as effective transmetalating agents. Complexes **Ir1–Ir6** were isolated as $PF_6^-$ salts, purified by recrystallization and characterized by $^1$H NMR (Figs. S1–S6), elemental analysis and ESI-MS (Figs. S7–S17). Moreover, the molecular structure of complex **Ir6** was also authenticated by X-ray crystallography (Fig. 1 and Tables S1–S2). These results suggested that the complexes were in good agreement with the expected structures. All complexes are scarcely soluble in water. However, they readily dissolve in $CH_3CN$, $CH_2Cl_2$, $CHCl_3$ and DMSO.

### 2.2. X-ray crystal structure

Crystals of complex **Ir6** were obtained by slow diffusion of hexane into a saturated solution of complex **Ir6** in $CH_2Cl_2/CHCl_3$ (1:1, v:v). The molecular structure for complex **Ir6** with atomic numbering scheme is shown in Fig. 1. X-ray crystallographic data and selected bond lengths and angles are summarized in Tables S1 and S2, respectively. The complex crystallized in the triclinic system with the *P*-1 space group. Complex **Ir6** adopt the expected half-sandwich pseudo-octahedral "three-legged piano-stool" geometry. The bond distance between the iridium center to the centroid of $Cp^{xbiph}$ ring is 1.8445 Å and the Ir—Cl bond distance is 2.397(3) Å. The ortho-metalated Ir—C bond distance [Ir–C = 2.014(8) Å] is slightly shorter than Ir—N bond distance [Ir–N = 2.121(7) Å]. Further, no intermolecular π-π stacking in the unit cell of complex **Ir6** is observed.

### 2.3. Study of the structure–activity relationship

To assess whether the present six imine-N-heterocyclic carbene ligands and their corresponding iridium(III) complexes possess cytotoxicity and potential structure–activity relationships (SARs), the in vitro cytotoxicity of ligands **L1–L6** and complexes **Ir1–Ir6** toward BEAS-2B human bronchial epithelial normal cells and A549 lung cancer cells were investigated after treatment for 24 h using the 3-(4,5-dimethylthiazol-2-yl)-2,5-diphenyltetrazoliumbromide (MTT) assay, with the well-known cisplatin as a positive control. The resulting 50% growth inhibitory concentration ($IC_{50}$) values are listed in Fig. 2 and Table 1. All of the imine-N-heterocyclic carbene ligands displayed exceedingly low cytotoxicity toward BEAS-2B cells and A549 cells (> 100 μM), they were thus deemed as inactive. Excitingly, this new class of complexes is highly potent against A549 cancer cells line with $IC_{50}$ values of 0.85–4.39 μM and display more high potency than the widely used clinical platinum drug cisplatin (21.3 μM). The cytotoxicity of these complexes may be derived from the combinatorial action of metal and imine-N-heterocyclic carbene ligands. Notably, complex **Ir6** was ca. 25 times as active as cisplatin in the A549 cell line (0.85 μM vs 21.3 μM), demonstrating great potential in cancer chemotherapy. Overall, the cytotoxic activities of complexes and cisplatin against A549 cancer cells are in the following order: **Ir6** > **Ir3** > **Ir5** > **Ir2** > **Ir1** > **Ir4** > cisplatin. In addition, to understand if the synthesized complexes are selective only against cancer cells, the human normal bronchial epithelial cells BEAS-2B was chosen to expound on the cytotoxicity of this family of complexes. The $IC_{50}$ values for complexes **Ir1–Ir6** toward BEAS-2B have been indicated in Table 1. Unfortunately, their selectivity toward cancer cells and normal cells was not observed. Therefore, more structural modification is necessary to reduce the cytotoxic activity toward normal cells without loss of the selectivity between cancer cells and normal cells in the future work.

The toxicological properties of this family of iridium(III) complexes can be governed via substitution effects of three tunable domains. First, when the length of the alkyl substitutions on the imidazole ring increased from methyl- to isopropyl-group, the complex display enhanced cytotoxicity (**Ir1**: 4.21 vs **Ir2**: 3.25 vs **Ir3**: 1.84 μM, **Ir3** > **Ir2** > **Ir1**). The increased tether length on the imidazole ring may increase the lipophilicity of this family of complexes and thus result in the enhanced cytotoxicity. Next, the anticancer activity can also be enhanced by increasing the size of *ortho*-substituents in aniline. For instance, under the same conditions as the other substituents ($R_1$ and $R_2$), complexes **Ir4** (4.39 μM) and **Ir5** (2.67 μM) exhibit in vitro anticancer activity dramatically surpass complexes **Ir2** (3.25 μM) and **Ir3** (1.84 μM), respectively. Ultimately, the effect of the substituent on the imine carbon on cytotoxicity of such complexes was further studied. When the substituent on imine carbon was changed from methyl to phenyl, the increased cytotoxic potency was observed (complex **Ir5**: $IC_{50}$ = 2.67 μM vs complex **Ir6**: $IC_{50}$ = 0.85 μM). Clearly, the anticancer properties of this class of complexes can be governed by subtle structure changing in

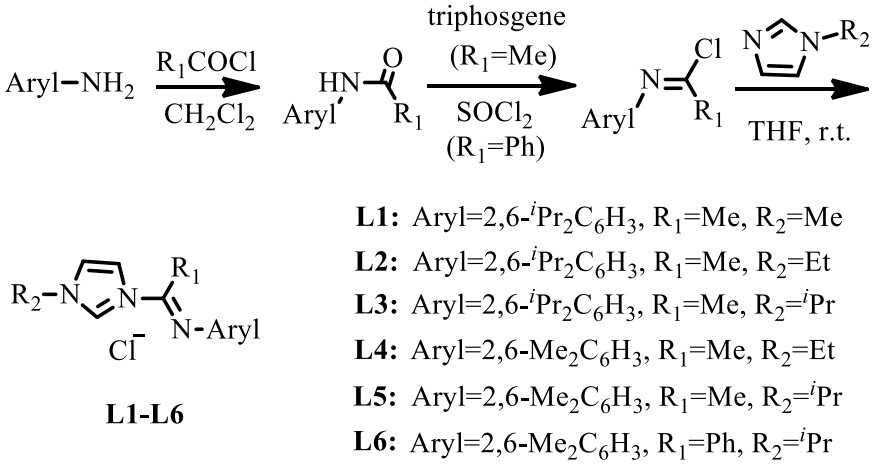


**Scheme 2.** Synthetic scheme of the imine-N-heterocyclic carbene ligands **L1**–**L6**.

cheating ligands. Previous studies have demonstrated that the cytotoxicity and lipophilicity of structurally similar half-sandwich iridium (III) anticancer complexes could be enhanced through the introduction of phenyl substituents on the Cp* ligand [40]. Within this class, the potency of these anticancer agents could be modulated by altering the lipophilicity of the substituents on three positions of the chelated ligands. These results build a structure–activity relationship for this type of half-sandwich iridium(III) complexes, which may be a rational strategy to design novel iridium(III) anticancer agents.

### 2.4. Reaction with NADH

In the human body, coenzyme NADH/$NAD^+$ play an essential role and participate in numerous metabolic reactions [41]. It has been reported that the similar half-sandwich iridium(III) anticancer agents as an efficient biocatalysts can oxidize NADH by hydride transfer to $O_2$ to yield reactive oxygen species (ROS) $H_2O_2$, which offered a pathway to an oxidant mechanism of action [42–44]. In order to explore the influence of three tunable domains on the catalytic ability in this class of new complexes, the time-dependent reactions of complexes **Ir1**–**Ir6** (ca. 1 μM) with NADH (100 μM) in 5% MeOH/95% $H_2O$ (v/v) were performed using ultraviolet-visible (UV–vis) spectrophotometer at 298 K (Fig. 3a and Fig. S18). The turnover numbers (TONs) of complexes **Ir1** (80.0), **Ir2** (85.0), **Ir3** (65.0), **Ir4** (70.0) **Ir5** (53.7) and **Ir6** (33.7) were computed by monitoring the absorbance change at 339 nm (Fig. 3b). Although no clear trends were observed, it appears that the substituent effects of three modifiable domains on the catalytic activity were pronounced. In particular, complex **Ir2** show ca. 8 times higher catalytic ability in the oxidation of NADH than the reported similarly half-sandwich iridium(III) complexes containing bis-NHC-based ligands under the same test conditions [45]. Thus, the strong catalytic ability of this family of complexes in converting NADH to $NAD^+$ may promote production of ROS and increase the anticancer potency in an oxidant mechanism of action.

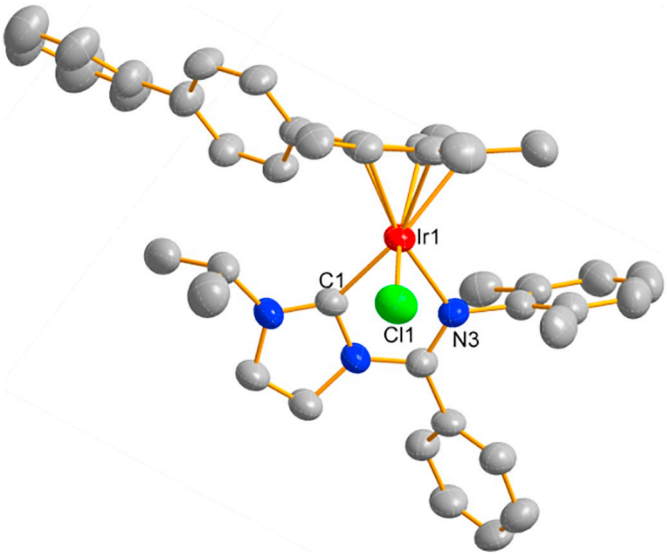


**Fig. 1.** X-ray crystal structure for complex **Ir6**. The hydrogen atoms and $PF_6^-$ counterions have been omitted for clarity. Selected bond lengths (Å) and angles (deg): Ir–C(centroid) = 1.8445, Ir–$C_{carbene}$ = 2.014(8), Ir–N = 2.121(7), Ir–Cl = 2.397(3), $C_{carbene}$–Ir–N = 76.1(3), $C_{carbene}$–Ir–Cl = 81.0(3), N–Ir–Cl = 88.2(2).

### 2.5. Interaction with model nucleobase

Complex **Ir6** was chosen as a representative to react with the DNA model 9-ethylguanine (9-EtG) and 9-methyladenine (9-MeA). The time-dependent reactions of complex **Ir6** with model nucleobase 9-EtG or 9-MeA were performed utilizing $^1$H NMR spectroscopy under the same conditions: complex **Ir6** (1 mM) in $CD_3OD$-$d_4$/$D_2O$ (8/2, v/v) with model nucleobase 9-EtG or 9-MeA (2 mM) tested from 5 min to 24 h at 310 K. As illustrated in Figs. S19 and S20, no new $^1$H NMR peaks were observed even after 24 h. Also, the formation of nucleobase adducts by

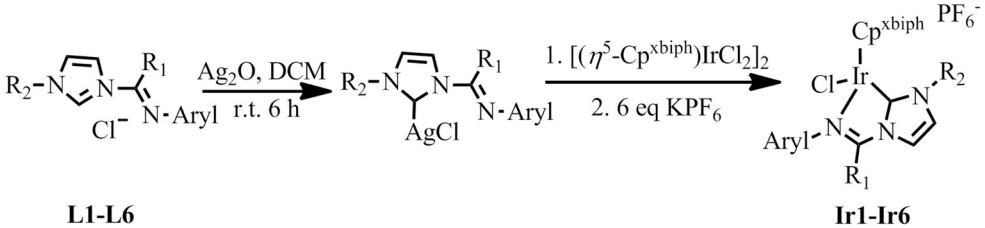


**Scheme 3.** Synthetic scheme of [($\eta^5$-$Cp^{xbiph}$)Ir(C^N)Cl]$PF_6^-$ complexes **Ir1**–**Ir6**.

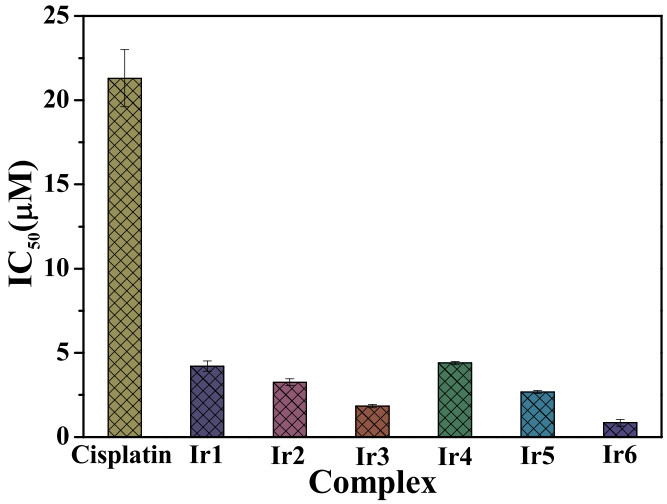


**Fig. 2.** Histogram showing the comparison of $IC_{50}$ values of complexes **Ir1–Ir6** and cisplatin toward A549 cancer cells after incubation for 24 h.

complex **Ir6** were not monitored using mass spectrometry. These results revealed that DNA may not be the target for this class of iridium(III) complexes.

### 2.6. Cell cycle arrest

Usually, most of the metal anticancer drugs inhibit the growth of cancer cells by disrupting the regulation of cell cycle distribution. To understand whether this class of complexes inhibited cell viability of A549 cells is on account of cell cycle arrest, cell cycle distribution of A549 cells was determined via quantitation of the DNA content. A549 cancer cells were treated with complex **Ir6** at concentrations of 0.25 × $IC_{50}$, 0.5 × $IC_{50}$, 1 × $IC_{50}$ and 2 × $IC_{50}$ for 24 h, then stained with propidium iodide (PI) and further analyzed by flow cytometry. As expected, the cell cycle distribution in A549 cells significantly changed, and the DNA content in $G_0/G_1$ phase increased from 51.16 ± 0.3% to 55.71 ± 0.6%, 57.27 ± 1.0%, 59.10 ± 1.0%, 61.45 ± 0.4% in a concentration-dependent manner after treatments with 0.25 × $IC_{50}$, 0.5 × $IC_{50}$, 1 × $IC_{50}$ and 2 × $IC_{50}$ of complex **Ir6**, respectively (Fig. 4, Fig. S21 and Table S3). These results indicated that complex **Ir6** strongly induced A549 cells to undergo $G_0/G_1$ phase arrest, which may be one of the possible mechanisms of cell growth inhibition.

### 2.7. Apoptosis assay

Apoptosis and necrosis are the two main types of cell death [46]. Previous studies have suggested that most anticancer drugs currently used in clinical trigger apoptosis in susceptible cells [47]. To understand the pathway potentially induced by complex **Ir6**, the Annexin V/propidium (PI) staining was employed to monitor the apoptosis of A549 cells. As illustrated in Fig. 5, Fig. S22 and Table S4, treatment of A549 cancer cells with complex **Ir6** at concentrations of 0.5 × $IC_{50}$ and 1 × $IC_{50}$ for 24 h, a concentrate-dependent apoptotic effect was observed. At the 1 × $IC_{50}$ tested concentration, complex **Ir6** caused early and late apoptosis in 13.48% and 20.85% of A549 cells, respectively, suggesting that the induction of cell death can occur through the apoptotic pathway.

### 2.8. Impact on mitochondrial membrane potential (MMP)

The loss of mitochondrial membrane potential (MMP, $\Delta\Psi_m$), an early event during apoptosis, is a significant indicator for the evaluation of apoptosis. The impact of complex **Ir6** on MMP was measured by staining with lipophilic cationic JC-1 dye. As shown in Fig. 6 and Table S5, with the concentration increases, a dose-dependent red-to-green color shift was observed, suggesting the decrease of MMP. The percentage of cells with mitochondrial membrane depolarization increases from 6.05% to 19.58% at a concentration of 1 × $IC_{50}$ compared to untreated cells. Hence, the dysfunction of mitochondria may contribute to the cytotoxic activity of this class of complexes.

### 2.9. Lysosomal damage

Lysosomes, an organelle in eukaryotic cells, control cell apoptosis or death at several levels, since they are involved in various aspects of cancer cell immortalization [48]. The lysosomal integrity is a crucial indicator for assess cell apoptosis or death. Acridine orange (AO) is a concentration-dependent fluorescent dye utilized to monitor the lysosomal integrity of A549 cells [49–51]. As shown in Fig. 7, a distinct decrease in red fluorescence intensity was observed as the concentration of complex **Ir6** increased, suggesting that the integrity of lysosomes was jeopardized, i.e., the increase of lysosomal permeabilization. Thus, we conclude that the cell apoptosis or death may depend on the disruption of lysosomes.

## 3. Conclusions

In conclusion, a set of half-sandwich iridium(III) complexes containing imine-N-heterocyclic carbene ligands were synthesized and characterized. These iridium(III) complexes exhibited highly potent cytotoxicity (up to 25-fold more effective than cisplatin) against A549 cancer cells. The substituent effects of three adjustable domains on cytotoxic potency were significant. The larger size of substituents on aniline and imidazole ring results in the higher anticancer efficiency. Additionally, introducing a more lipophilic phenyl ring also enhances the anticancer activity of the complexes. These complexes have strong catalytic ability in the oxidation of NADH. However, no clear trend was observed for the substituent effects of three adjustable domains on the catalytic ability. No binding to 9-EtG or 9-MeA was observed for this

**Table 1**
Test data of $IC_{50}$ values for ligands **L1–L6**, complexes **Ir1–Ir6** and cisplatin[a] toward A549 lung cancer cells and BEAS-2B human bronchial epithelial normal cells.

| Ligand | $IC_{50}$ (μM) | | Complex | $IC_{50}$ (μM) | |
|---|---|---|---|---|---|
| | A549 | BEAS-2B | | A549 | BEAS-2B |
| **L1** | > 100 | > 100 | $[(\eta^5\text{-Cp}^{xbiph})Ir(L1)Cl]PF_6$ (**Ir1**) | 4.21 ± 0.3 | 3.58 ± 0.3 |
| **L2** | > 100 | > 100 | $[(\eta^5\text{-Cp}^{xbiph})Ir(L2)Cl]PF_6$ (**Ir2**) | 3.25 ± 0.2 | 2.03 ± 0.2 |
| **L3** | > 100 | > 100 | $[(\eta^5\text{-Cp}^{xbiph})Ir(L3)Cl]PF_6$ (**Ir3**) | 1.84 ± 0.1 | 0.60 ± 0.3 |
| **L4** | > 100 | > 100 | $[(\eta^5\text{-Cp}^{xbiph})Ir(L4)Cl]PF_6$ (**Ir4**) | 4.39 ± 0.1 | 3.43 ± 0.1 |
| **L5** | > 100 | > 100 | $[(\eta^5\text{-Cp}^{xbiph})Ir(L5)Cl]PF_6$ (**Ir5**) | 2.67 ± 0.1 | 1.21 ± 0.3 |
| **L6** | > 100 | > 100 | $[(\eta^5\text{-Cp}^{xbiph})Ir(L6)Cl]PF_6$ (**Ir6**) | 0.85 ± 0.2 | 4.60 ± 0.5 |
| | | | Cisplatin | 21.3 ± 1.7 | 42.0 ± 2.3 |

Data are presented as means ± standard deviations and cell viability is assessed after 24 h of incubation.
[a] $IC_{50}$ values are drug concentrations necessary for 50% inhibition of cell viability.

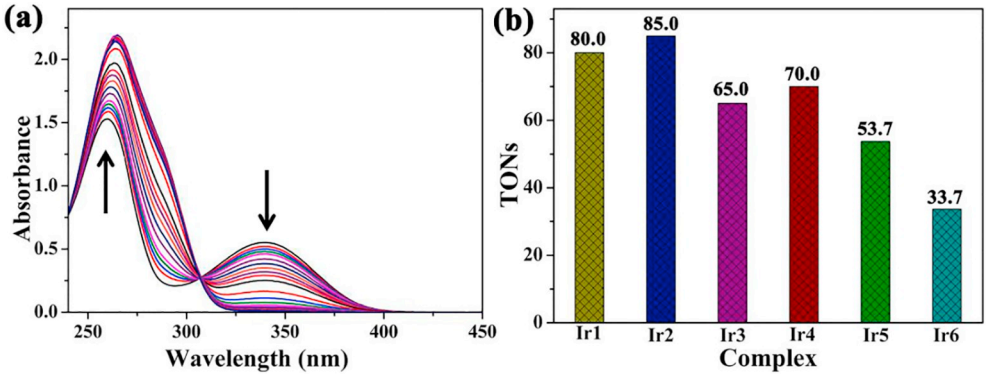


**Fig. 3.** (a) UV–vis spectra of the reaction of NADH (100 μM) with complex **Ir2** (1 μM) in 5% MeOH/95% $H_2O$ (v:v) at 298 K for 8 h; (b) The turnover numbers (TONs) of complexes **Ir1**–**Ir6**.

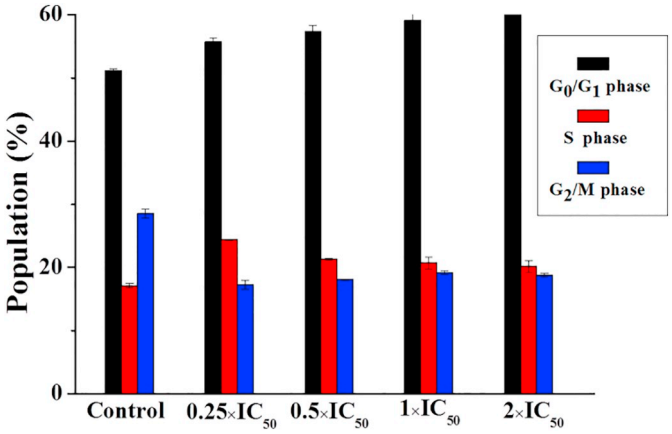


**Fig. 4.** Flow cytometry data for cell cycle distribution of A549 cancer cells exposed to complex **Ir6** for 24 h. Concentrations used were 0.25, 0.5, 1 and 2 equipotent concentrations of $IC_{50}$. Cell staining for flow cytometry was carried out using PI/RNase. Data are quoted as mean ± SD of three replicates.

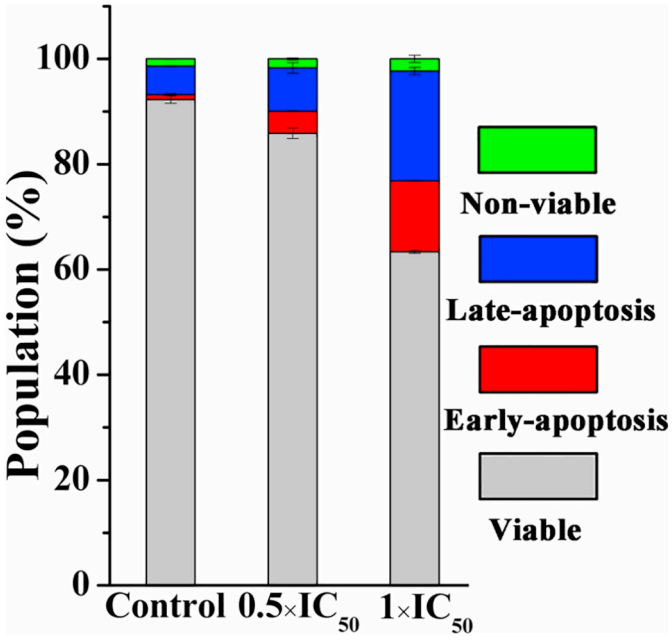


**Fig. 5.** Apoptosis analysis of A549 cells after 24 h of exposure to complex **Ir6** at 310 K determined by flow cytometry using annexin V-FITC vs PI staining. Populations for cells in four stages treated by complex **Ir6**. Data are quoted as mean ± SD of three replicates.

type of complexes. Flow cytometric analysis showed that complex **Ir6** can stall cell in the $G_0/G_1$ phase of the cell cycle, lead to loss of the MMP and trigger early- and late-stage apoptosis in A549 cells. Interestingly, lysosomal damage was detected in A549 cancer cells utilizing confocal microscopy. These initial studies point out that the half-sandwich iridium(III) complexes in this system possess some interesting biological effects and worthy of further investigation.

## 4. Experimental section

### 4.1. General information

2,3,4,5-Tetramethyl-2-cyclopentenone (95%), butyllithium solution (1.6 M in hexane), 4-bromo-biphenyl, $IrCl_3{\cdot}nH_2O$, 2,6-dimethylaniline, 2,6-diisopropylaniline, acetyl chloride, benzoyl chloride, triphosgene, thionyl chloride, 1-methylimidazole, 1-ethylimidazole, 1-isopropylimidazole, $Ag_2O$, 9-ethylguanine and 9-methyladenine were purchased from commercial source. $[(\eta^5\text{-}C_5Me_4C_6H_4C_6H_5)IrCl_2]_2$ was synthesized according to previously reported methods [40]. The intermediate compounds were prepared according to previously reported procedure [52–57]. The ligands **L1–L5** [52], **L6** [53–57] were prepared according to slightly modified literature procedure, respectively.

$^1H$ NMR spectra were acquired at 298 K on Bruker DPX 500 spectrometers using TMS as an internal standard and $CDCl_3$ as solvent. Mass spectra of the ligands were recorded on a Thermo LTQ Orbitrap XL ($ESI^+$). Mass spectra of the complexes were recorded on a Atouflex Speed MALDI-TOF MS. X-ray Diffraction data were obtained on a Bruker Smart CCD area detector with graphite-monochromated Mo Kα radiation (λ = 0.71073 Å).

### 4.2. Synthesis of $[(\eta^5\text{-}Cp^{xbiph})Ir(C\hat{}N)Cl]PF_6$

A round-bottomed flask was charged with a mixture of ligands (0.10 mmol) and $Ag_2O$ (1.2 eq) in $CH_2Cl_2$ (20 mL) were stirred at room temperature for 6 h. The mixture was filtered through Celite. The filtrate was charged with $[(\eta^5\text{-}Cp^{xbiph})IrCl_2]Cl_2$ (0.05 mmol). The mixture was then stirred at room temperature for 12 h. Subsequently, $KPF_6$ (6 eq) was added and further stir for 30 min. The suspension was filtered and the solvent was removed using vacuum system. The orange solid was obtained by recrystallizing from $CH_2Cl_2$ and hexane solution.

**Ir1** Yield: 77.1 mg (83%). $^1H$ NMR (500 MHz, $CDCl_3$) $\delta$ 7.68 (d, $J$ = 2.3 Hz, 1H), 7.65 (d, $J$ = 8.2 Hz, 2H), 7.61 (d, $J$ = 7.4 Hz, 2H), 7.46 (t, $J$ = 7.6 Hz, 2H), 7.38 (t, $J$ = 7.4 Hz, 1H), 7.35 (s, 1H), 7.34–7.29 (m, 4H), 7.17 (dd, $J$ = 6.2, 3.0 Hz, 1H), 3.73 (s, 3H), 3.61–3.52 (m, 1H), 2.53 (s, 3H), 2.38–2.29 (m, 1H), 1.87 (s, 3H), 1.64 (s, 3H), 1.51 (s, 3H), 1.35 (s, 3H), 1.19 (d, $J$ = 6.6 Hz, 3H), 0.97 (d, $J$ = 6.7 Hz, 6H), 0.68 (d, $J$ = 6.5 Hz, 3H). ESI-MS ($m/z$): calcd for $C_{39}H_{46}IrClN_3$: 784.301, found: 784.295, $[(\eta^5\text{-}C_5Me_4C_6H_4C_6H_5)Ir(L1)Cl]^+$. Elemental analysis: calcd (%) for $C_{39}H_{46}N_3IrClPF_6$: C, 50.40; H, 4.99; N, 4.52; found: C, 50.56; H,

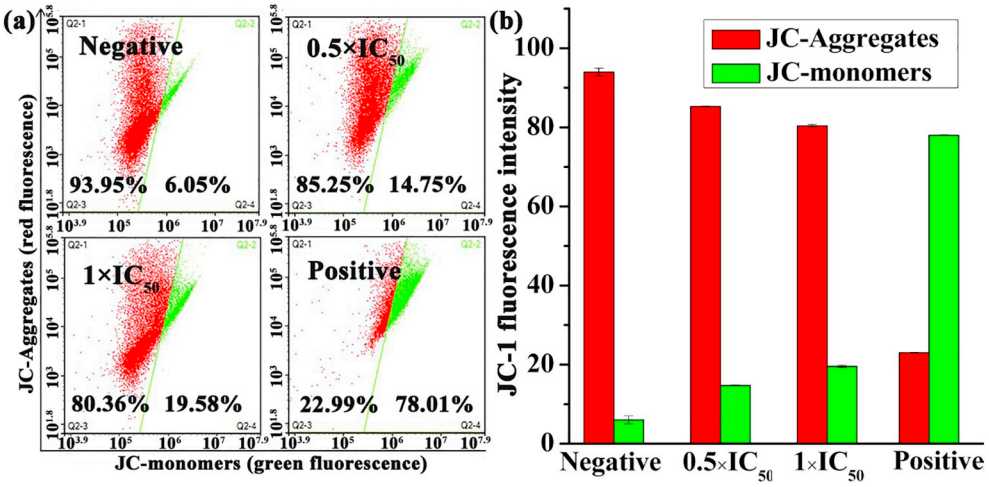


**Fig. 6.** Complex **Ir6** induced mitochondrial membrane potential changes in A549 cells.

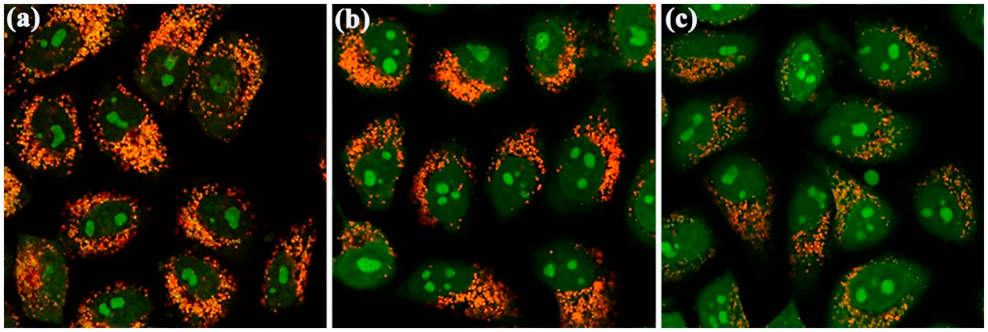


**Fig. 7.** Observation of lysosomal disruption in A549 cells loaded with complex **Ir6** for 6 h at 37 °C, then stained with acridine orange (AO) (5 μM) at 37 °C for 15 min. Emission was collected at 510 ± 20 nm (green) and 625 ± 20 nm (red) upon excitation at 488 nm. The A549 cells were treated with (a) only acridine orange (AO); (b) acridine orange (AO) and complex **Ir6** (1 × $IC_{50}$); (c) acridine orange (AO) and complex **Ir6** (3 × $IC_{50}$). Scale bar: 20 μm.

4.94; N, 4.69.

**Ir2** Yield: 83.3 mg (88%). $^1$H NMR (500 MHz, $CDCl_3$) $\delta$ 7.73 (d, $J$ = 2.2 Hz, 1H), 7.67 (d, $J$ = 8.1 Hz, 2H), 7.62 (d, $J$ = 7.3 Hz, 2H), 7.47 (t, $J$ = 7.6 Hz, 2H), 7.39 (d, $J$ = 7.4 Hz, 1H), 7.36 (d, $J$ = 8.5 Hz, 2H), 7.34–7.29 (m, 3H), 7.20 (dd, $J$ = 6.5, 2.7 Hz, 1H), 4.00 (dq, $J$ = 14.4, 7.2 Hz, 1H), 3.90 (dq, $J$ = 14.6, 7.4 Hz, 1H), 3.63–3.55 (m, 1H), 2.55 (s, 3H), 2.45–2.36 (m, 1H), 1.83 (s, 3H), 1.62 (s, 3H), 1.47 (s, 3H), 1.41 (d, $J$ = 2.4 Hz, 3H), 1.39 (d, $J$ = 7.3 Hz, 3H), 1.20 (d, $J$ = 6.6 Hz, 3H), 1.01 (d, $J$ = 6.6 Hz, 3H), 0.98 (d, $J$ = 6.8 Hz, 3H), 0.78 (d, $J$ = 6.4 Hz, 3H). ESI-MS ($m/z$): calcd for $C_{40}H_{48}IrClN_3$: 798.3166, found: 798.2949, $[(\eta^5\text{-}C_5Me_4C_6H_4C_6H_5)Ir(L2)Cl]^+$. Elemental analysis: calcd (%) for $C_{40}H_{48}N_3IrClPF_6$: C, 50.92; H, 5.13; N, 4.45; found: C, 50.78; H, 5.30; N, 4.58.

**Ir3** Yield: 67.2 mg (70%). $^1$H NMR (500 MHz, $CDCl_3$) $\delta$ 7.79 (s, 1H), 7.69 (d, $J$ = 7.8 Hz, 2H), 7.61 (d, $J$ = 7.6 Hz, 2H), 7.47 (t, $J$ = 7.6 Hz, 2H), 7.40 (dd, $J$ = 13.0, 7.1 Hz, 3H), 7.36–7.31 (m, 2H), 7.30 (s, 1H), 7.22 (dd, $J$ = 6.8, 2.4 Hz, 1H), 4.33–4.22 (m, 1H), 3.64–3.55 (m, 1H), 2.56 (s, 3H), 2.52–2.41 (m, 1H), 1.82 (s, 3H), 1.58 (s, 3H), 1.45 (d, $J$ = 12.0 Hz, 6H), 1.38 (dd, $J$ = 6.4, 4.4 Hz, 6H), 1.20 (d, $J$ = 6.6 Hz, 3H), 1.04 (d, $J$ = 6.3 Hz, 3H), 0.98 (d, $J$ = 6.8 Hz, 3H), 0.86 (d, $J$ = 6.2 Hz, 3H). ESI-MS ($m/z$): calcd for $C_{41}H_{50}IrClN_3$: 812.332, found: 812.317, $[(\eta^5\text{-}C_5Me_4C_6H_4C_6H_5)Ir(L3)Cl]^+$. Elemental analysis: calcd (%) for $C_{41}H_{50}N_3IrClPF_6$: C, 51.43; H, 5.26; N, 4.39; found: C, 51.62; H, 5.33; N, 4.61.

**Ir4** Yield: 59.4 mg (67%). $^1$H NMR (500 MHz, $CDCl_3$) $\delta$ 7.69 (d, $J$ = 8.2 Hz, 3H), 7.66–7.62 (m, 2H), 7.53 (d, $J$ = 8.1 Hz, 2H), 7.47 (t, $J$ = 7.6 Hz, 2H), 7.39 (t, $J$ = 7.4 Hz, 1H), 7.26–7.23 (m, 1H), 7.21 (t, $J$ = 4.1 Hz, 2H), 7.18 (d, $J$ = 2.1 Hz, 1H), 3.73–3.62 (m, 2H), 2.57 (s, 3H), 2.29 (s, 3H), 2.06 (s, 3H), 1.83 (s, 3H), 1.73 (s, 3H), 1.35 (s, 3H), 1.21 (t, $J$ = 7.3 Hz, 3H), 1.18 (s, 3H). ESI-MS ($m/z$): calcd for $C_{36}H_{40}IrClN_3$: 742.2540, found: 742.2304, $[(\eta^5\text{-}C_5Me_4C_6H_4C_6H_5)Ir(L4)Cl]^+$. Elemental analysis: calcd (%) for $C_{36}H_{40}N_3IrClPF_6$: C, 48.73; H, 4.54; N, 4.74; found: C, 48.90; H, 4.60; N, 4.78.

**Ir5** Yield: 70.1 mg (78%). $^1$H NMR (500 MHz, $CDCl_3$) $\delta$ 7.80 (s, 1H), 7.69 (d, $J$ = 8.2 Hz, 2H), 7.61 (d, $J$ = 7.5 Hz, 2H), 7.56 (d, $J$ = 8.1 Hz, 2H), 7.47 (t, $J$ = 7.6 Hz, 2H), 7.39 (t, $J$ = 7.3 Hz, 1H), 7.25–7.19 (m, 3H), 7.17 (d, $J$ = 2.3 Hz, 1H), 4.07–3.99 (m, 1H), 2.58 (s, 3H), 2.28 (s, 3H), 2.06 (s, 3H), 1.83 (s, 3H), 1.76 (s, 3H), 1.29 (s, 3H), 1.21 (d, $J$ = 6.7 Hz, 3H), 1.19 (s, 3H), 1.15 (d, $J$ = 6.7 Hz, 3H). ESI-MS ($m/z$): calcd for $C_{37}H_{42}IrClN_3$: 756.2697, found: 756.2418, $[(\eta^5\text{-}C_5Me_4C_6H_4C_6H_5)Ir(L5)Cl]^+$. Elemental analysis: calcd (%) for $C_{37}H_{42}N_3IrClPF_6$: C, 49.30; H, 4.70; N, 4.66; found: C, 49.48; H, 4.90; N, 4.77.

**Ir6** Yield: 52.6 mg (55%). $^1$H NMR (500 MHz, $CDCl_3$) $\delta$ 8.11 (s, 1H), 7.76 (d, $J$ = 8.1 Hz, 2H), 7.71 (d, $J$ = 8.1 Hz, 2H), 7.65 (d, $J$ = 7.7 Hz, 2H), 7.60 (s, 1H), 7.52–7.44 (m, 3H), 7.39 (t, $J$ = 7.3 Hz, 1H), 7.27 (d, $J$ = 3.9 Hz, 1H), 7.20 (s, 1H), 7.15 (d, $J$ = 7.5 Hz, 1H), 7.11 (d, $J$ = 1.8 Hz, 1H), 7.03 (dd, $J$ = 13.8, 6.2 Hz, 2H), 6.93 (d, $J$ = 7.5 Hz, 1H), 4.17–4.05 (m, 1H), 2.55 (s, 3H), 1.92 (s, 6H), 1.88 (s, 3H), 1.32–1.15 (m, 12H). ESI-MS ($m/z$): calcd for $C_{42}H_{44}IrClN_3$: 818.285, found: 818.323, $[(\eta^5\text{-}C_5Me_4C_6H_4C_6H_5)Ir(L6)Cl]^+$. Elemental analysis: calcd (%) for $C_{42}H_{44}N_3IrClPF_6$: C, 52.36; H, 4.60; N, 4.36; found: C, 52.59; H, 4.83; N, 4.49. Single crystals were obtained by slow diffusion of hexane into a mixture solution of $CH_2Cl_2$ and $CHCl_3$ (v:v, 1:1).

## Abbreviations

| | |
|---|---|
| $Cp^{xbiph}$ | tetramethyl(biphenyl)cyclopentadienyl |
| NHCs | N-heterocyclic carbenes |
| HSA | human serum albumin |
| MoAs | mechanisms of action |
| EGFR | epidermal growth factor receptor |
| 9-EtG | 9-ethylguanine |
| 9-MeA | 9-methyladenine |

| | |
|---|---|
| $IC_{50}$ | 50% growth inhibitory concentration |
| BSA | bovine serum albumin |
| GSH | glutathione |
| SARs | structural-activity relationships |
| ROS | reactive oxygen species |
| AO | acridine orange |
| MMP | mitochondrial membrane potential |
| UV–vis | ultraviolet-visible |

## Acknowledgements

We are grateful for the supports of the Shandong Provincial Natural Science Foundation (ZR2018MB023), the National Natural Science Foundation of China (Grant No. 21671118) and the Taishan Scholars Program, the Key Laboratory of Polymeric Composite & Functional Materials of Ministry of Education (PCFM-2017-01), excellent experiment project of Qufu Normal University (jp201705).

## Appendix A. Supplementary data

Supplementary data to this article can be found online at https://doi.org/10.1016/j.jinorgbio.2018.11.007.

## References

[1] E.R. Jamieson, S.J. Lippard, Chem. Rev. 99 (1999) 2467–2498.
[2] G. Chu, J. Biol. Chem. 269 (1994) 787–790.
[3] V. Cepeda, M.A. Fuertes, J. Castilla, C. Alonso, C. Quevedo, J.M. Pérez, Anti Cancer Agents Med. Chem. 7 (2007) 3–18.
[4] L. Kelland, Nat. Rev. Cancer 7 (2007) 573–584.
[5] R.P. Miller, R.K. Tadagavadi, G. Ramesh, W.B. Reeves, Toxins 2 (2010) 2490–2518.
[6] Y.R. Zheng, K. Suntharalingam, T.C. Johnstone, H. Yoo, W. Lin, J.G. Brooks, S.J. Lippard, J. Am. Chem. Soc. 136 (2014) 8790–8798.
[7] A.M. Florea, D. Büsselberg, Cancers 3 (2011) 1351–1371.
[8] Z.Z. Tian, J.J. Li, S.M. Zhang, Z.S. Xu, Y.L. Yang, D.L. Kong, H.R. Zhang, X.X. Ge, J.M. Zhang, Z. Liu, Inorg. Chem. 57 (2018) 10498–10502.
[9] M. Tian, J.J. Li, S.M. Zhang, L.H. Guo, X.D. He, D.L. Kong, H.R. Zhang, Z. Liu, Chem. Commun. 53 (2017) 12810–12813.
[10] Q. Du, L.H. Guo, M. Tian, X.X. Ge, Y.L. Yang, X.Y. Jian, Z.S. Xu, Z.Z. Tian, Z. Liu, Organometallics 37 (2018) 2880–2889.
[11] L.L. Zeng, P. Gupta, Y.L. Chen, E.J. Wang, L.N. Ji, H. Chao, Z.S. Chen, Chem. Soc. Rev. 46 (2017) 5771–5804.
[12] T.T. Zou, C.T. Lum, C.N. Lok, J.J. Zhang, C.M. Che, Chem. Soc. Rev. 44 (2015) 8786–8801.
[13] M. Li, L.H. Lai, Z.N. Zhao, T.F. Chen, Chem. Asian J. 11 (2016) 310–320.
[14] Z.Q. Zhang, X.Y. Wang, C. Luo, C.C. Zhu, K. Wang, C.L. Zhang, Z.J. Guo, Chem. Asian J. 12 (2017) 1659–1667.
[15] L.J. Liu, W.H. Wang, S.Y. Huang, Y.J. Hong, G.D. Li, S. Lin, J.L. Tian, Z.W. Cai, H.M.D. Wang, D.L. Ma, C.H. Leung, Chem. Sci. 8 (2017) 4756–4763.
[16] J. Arshad, M. Hanif, S. Movassaghi, M. Kubanik, A. Waseem, T. Söhnel, S.M.F. Jamieson, C.G. Hartinger, J. Inorg. Biochem. 177 (2017) 395–401.
[17] Q. Du, Y.L. Yang, L.H. Guo, M. Tian, X.X. Ge, Z.Z. Tian, L.P. Zhao, Z.S. Xu, J.J. Li, Z. Liu, Dyes Pigments (2018), https://doi.org/10.1016/j.dyepig.2018.11.009.
[18] L. Biancalana, L.K. Batchelor, T. Funaioli, S. Zacchini, M. Bortoluzzi, G. Pampaloni, P.J. Dyson, F. Marchetti, Inorg. Chem. 57 (2018) 6669–6685.
[19] Q. Wu, L.Y. Liu, S.L. Li, F.X. Wang, J. Li, Y. Qian, Z. Su, Z.W. Mao, P.J. Sadler, H.K. Liu, J. Inorg. Biochem. 189 (2018) 30–39.
[20] W.L. Ma, Z.Z. Tian, S.M. Zhang, X.D. He, J.J. Li, X.R. Xia, X.B. Chen, Z. Liu, Inorg. Chem. Front. 5 (2018) 2587–2597.
[21] Y.L. Yang, L.H. Guo, Z.Z. Tian, Y.T. Gong, H.M. Zheng, S.M. Zhang, Z.S. Xu, X.X. Ge, Z. Liu, Inorg. Chem. 57 (2018) 11087–11098.
[22] K.G. Samper, S.C. Marker, P. Bayón, S.N. MacMillan, I. Keresztes, Ò. Palacios, J.J. Wilson, J. Inorg. Biochem. 177 (2017) 335–343.
[23] L.H. Guo, H.R. Zhang, M. Tian, Z.Z. Tian, Y.J. Xu, Y.L. Yang, H.W. Peng, P. Liu, Z. Liu, New J. Chem. 42 (2018) 16183–16192.
[24] M. Ouyang, L.L. Zeng, H.Y. Huang, C.Z. Jin, J.P. Liu, Y. Chen, L.N. Ji, H. Chao, Dalton Trans. 46 (2017) 6734–6744.
[25] Y. Li, B. Liu, X.R. Lu, M.F. Li, L.N. Ji, Z.W. Mao, Dalton Trans. 46 (2017) 11363–11371.
[26] W.A. Herrmann, Angew. Chem. Int. Ed. 41 (2002) 1290–1309.
[27] L.H. Guo, S.Y. Dai, X.L. Sui, C.L. Chen, ACS Catal. 6 (2016) 428–441.
[28] Y. Li, C.P. Tan, W. Zhang, L. He, L.N. Ji, Z.W. Mao, Biomaterials 39 (2015) 95–104.
[29] Y.L. Yang, L.H. Guo, Z.Z. Tian, X.C. Liu, Y.T. Gong, H.M. Zheng, X.X. Ge, Z. Liu, Chem. Asian J. 13 (2018) 2923–2933.
[30] L.H. Guo, C.L. Chen, Sci. China Chem. 58 (2015) 1663–1673.
[31] S. Díez-González, N. Marion, S.P. Nolan, Chem. Rev. 109 (2009) 3612–3676.
[32] L.H. Guo, W.J. Liu, C.L. Chen, Mater. Chem. Front. 1 (2017) 2487–2494.
[33] Y.L. Yang, L.H. Guo, X.X. Ge, Z.Z. Tian, Y.T. Gong, H.M. Zheng, Q. Du, X.F. Zheng, Z. Liu, Dyes Pigments 161 (2019) 119–129.
[34] T.T. Fong, C.N. Lok, C.Y. Chung, Y.E. Fung, P.K. Chow, P.K. Wan, C.M. Che, Angew. Chem. Int. Ed. 55 (2016) 11935–11939.
[35] Y. Li, G.F. Liu, C.P. Tan, L.N. Ji, Z.W. Mao, Metallomics 6 (2014) 1460–1468.
[36] Y. Gothe, T. Marzo, L. Messori, N. Metzler-Nolte, Chem. Commun. 51 (2015) 3151–3153.
[37] W. Streciwilk, A. Terenzi, X. Cheng, L. Hager, Y. Dabiri, P. Prochnow, J.E. Bandow, S. Wölfl, B. Keppler, I. Ott, Eur. J. Med. Chem. 156 (2018) 148–161.
[38] R.W. Sun, L.F. Chow, X.H. Li, J.J. Yan, S.Y. Chui, C.M. Che, Chem. Sci. 2 (2011) 728–736.
[39] D. Jantke, M. Cokoja, A. Pöthig, W.A. Herrmann, F.E. Kühn, Organometallics 32 (2013) 741–744.
[40] Z. Liu, A. Habtemariam, A.M. Pizarro, S.A. Fletcher, A. Kisova, O. Vrana, L. Salassa, P.C.A. Bruijnincx, G.J. Clarkson, V. Brabec, P.J. Sadler, J. Med. Chem. 54 (2011) 3011–3026.
[41] F.S. Omar, N. Duraisamy, K. Ramesh, S. Ramesh, Biosens. Bioelectron. 79 (2016) 763–775.
[42] Z. Liu, I. Romero-Canelón, B. Qamar, J.M. Hearn, A. Habtemariam, N.P.E. Barry, A.M. Pizarro, G.J. Clarkson, P.J. Sadler, Angew. Chem. 126 (2014) 4022–4027.
[43] H.R. Zhang, L.H. Guo, Z.Z. Tian, M. Tian, S.M. Zhang, Z.S. Xu, P.W. Gong, X.F. Zheng, J. Zhao, Z. Liu, Chem. Commun. 54 (2018) 4421–4424.
[44] Z. Liu, P.J. Sadler, Acc. Chem. Res. 47 (2014) 1174–1185.
[45] C.L. Wang, J.F. Liu, Z.Z. Tian, M. Tian, L.J. Tian, W.Q. Zhao, Z. Liu, Dalton Trans. 46 (2017) 6870–6883.
[46] I. Vermes, C. Haanen, Adv. Clin. Chem. 31 (1994) 177–246.
[47] N.A. Thornberry, Y. Lazebnik, Science 281 (1998) 1312–1316.
[48] M.T. Gyparaki, A.G. Papavassiliou, Trends Mol. Med. 20 (2014) 239–241.
[49] X.Z. Zhao, M.L. Li, W. Sun, J.L. Fan, J.J. Du, X.J. Peng, Chem. Commun. 54 (2018) 7038–7041.
[50] L. He, Y. Li, C.P. Tan, R.R. Ye, M.H. Chen, J.J. Cao, L.N. Ji, Z.W. Mao, Chem. Sci. 6 (2015) 5409–5418.
[51] P. Boya, G. Kroemer, Oncogene 27 (2008) 6434–6451.
[52] J.A. Deng, H.Y. Gao, F.M. Zhu, Q. Wu, Organometallics 32 (2013) 4507–4515.
[53] M. Frøseth, K.A. Netland, C. Rømming, M. Tilset, J. Organomet. Chem. 690 (2005) 6125–6132.
[54] M.L. Rosenberg, A. Krivokapic, M. Tilset, Org. Lett. 11 (2009) 547–550.
[55] M.L. Rosenberg, E. Langseth, A. Krivokapic, N.S. Gupta, M. Tilset, New J. Chem. 35 (2011) 2306–2313.
[56] A. Krajete, G. Steiner, H. Kopacka, K.H. Ongania, K. Wurst, M.O. Kristen, P. Preishuber-Pflügl, B. Bildstein, Eur. J. Inorg. Chem. (8) (2004) 1740–1752.
[57] S. Dastgir, K.S. Coleman, A.R. Cowley, M.L.H. Green, Organometallics 25 (2006) 300–306.